Transient response of a concrete tunnel in an elastic rock with imperfect contact

R. Shakeri, A. Mesgouez, G. Lefeuve-Mesgouez

Version of Record: https://www.sciencedirect.com/science/article/pii/S2095268619302423
Manuscript_3261af03004eb8e42e260915d244441a

Transient response of a concrete tunnel in an elastic rock with imperfect contact

R. Shakeri[a,b], A. Mesgouez[a,*], G. Lefeuve-Mesgouez[a]

[a] *UMR 1114 EMMAH, Avignon University, F-84916 Avignon, France*
[b] *Department of Civil, Environmental & Architectural Engineering, University of Colorado Boulder, CO 80309, USA*

Abstract: The two-dimensional transient response of an imperfect bonded circular lined pipeline lying in an elastic infinite medium is investigated. Imperfect boundary conditions between the surrounding elastic rock and the tunnel are modelled with a two-linear-spring design. The novelty of the manuscript consists in studying at the same time transient regimes and imperfect bonded interfaces for simulating the dynamic response of a tunnel embedded in an elastic infinite rock. Wave propagation fields in tunnel and rock are expressed in terms of infinite Bessel and Hankel series. To solve the transient problem, the Laplace transform and the associated Durbin's algorithm are performed. To exhibit the dynamic responses, influences of various parameters such as the quality of the interface conditions and the thickness of the lining are presented. The dynamic hoop stresses and the solid displacements of both the tunnel and the rock are also proposed.

Keywords: Dynamic response; Imperfect interface; Circular tunnel; Semi-analytical approach; Transient wave propagation

1. Introduction

The effect of underground structures on surrounding environments and the effect of surrounding environments on underground structures are of great importance in various fields such as civil engineering constructions, mining or geophysics. More specifically, studying wave propagation in complex heterogeneous media e.g. ground structures is useful not only for geotechnical and mechanical applications or seismic events, but also for medium characterisation since wave propagation signals contain information on the medium itself. Various techniques use for instance the determination of electrical resistivity properties or/and mechanical wave speeds from first arrival times to characterise heterogeneous grounds. Such methods have been applied in the specific underground environment of the LSBB (Low Noise Inter-Disciplinary Underground Science and Technology Laboratory, situated in Rustrel, Vaucluse, southern France), which is constituted of a system of galleries with or without concrete layers [1]. It belongs to the Albion plateau, a karstic limestone unit of the southern French Alps. With the aim of better characterising the configuration of the LSBB, a new strategy is proposed and the methodology, based on a mechanical wave propagation modelling and especially the study of the full waveform signal, will follow three main steps in a long term process: (1) implementation of a robust and efficient forward problem, in relation with the LSBB configuration geometry that focuses on the transient responses in terms of stress and displacement fields (short term); (2) a sensitivity analysis [2] to extract the main influential mechanical parameters in the LSBB configuration (medium term); and (3) an adequate inversion process related to the latest mechanical parameters and with a full waveform inversion approach to take into account the entire content of the transient response and thus as much information as possible (long term) [3-5]. The paper focuses here on the first part of the project. Resulting from different recent observations, it has been noticed that the concrete layer does not present everywhere a perfect contact with the surrounding rock. Moreover, the digging of the tunnel has weakened some parts of the massif, and a damaged zone has appeared in several areas. It appears then to be important to take into account in the model different kinds of contacts, and to study their effects. A bibliographical review shows that wave propagation modelling can still be improved by taking into account more realistic boundary conditions between the massif and the tunnel for transient excitations. Beyond the specific objective of our study, the work proposed here can also be considered for other applications such as modelling seismic wave propagation in fluid-filled boreholes [6], deeply buried pipelines subjected to hydraulic fracture initiation or internal blast loads [7,8], safety of tunnels during earthquakes [9].

Received 20 May 2019
Received in revised form 10 March 2020
* Corresponding author.
E-mail address: arnaud.mesgouez@univ-avignon.fr

In the transient regime, researchers have employed numerical methods such as a combination of finite element method (FEM) and boundary element method (BEM) [10,11] or BEM [12-16] to study the transient wave scattering of cavities or tunnels in half and full space environments and its effect on ground surface and tunnel's responses. Concerning the semi-analytical developments for dynamic studies, Kouretzis et al. developed an analytical methodology to calculate the strain field in buried pipelines due to surface blast load [17]. The 3D cylindrical thin shell theory was considered and the authors focused on the analytical results of strain analysis of P- and Rayleigh waves. A good comparison with experimental results and numerical FEM results was achieved. The 3D and transient response of an explosion occurring inside a buried pipeline was also studied by Feldgun et al. who used the Timoshenko elastic plastic shell theory for the pipeline and a Grigoryan model for the soil [18]. Smerzini et al. focused on the effects of underground structures, such as circular cavity or elastic shell, on the surface motion of a 2D homogeneous, isotropic and linear viscoelastic half-space subjected to seismic SH excitation in frequency and time domains [19]. The theoretical approach is based on the expansion of wave functions in terms of Bessel and Hankel functions. Nonlinear dynamic response of functionally graded shells resting on elastic foundations for various geometries [20-22] has been performed with several classical shell theories, studying particularly the elastic foundation influence on the vibration of functionally graded materials. Kouretzis et al. established a closed-form solution to calculate tunnel forces due to P-wave propagation in an elastic medium under full-slip conditions and showed that P-waves can lead to higher axial hoop forces compared to S-waves [23]. Zhai et al. studied the effect of a cylindrical cavity buried in an elastic soil subjected to an anti-plane Heaviside step load [24]. They solved the equations in the Laplace transform domain and the inverse transform was calculated using contour integration techniques along an appropriate integration path. Comparisons both with static results and with Durbin's method were proposed. Fu et al. used indirect boundary element method with Green's function of distributed loads to study soil-tunnel interaction of a rigid tunnel buried in an elastic multilayered soil (an elastic layer over an elastic bedrock) [25].

Beside the transient aspect of the response, one of the most influential parameters for the dynamic response of the mechanical tunnel is the quality of the interface between the rock and the tunnel. Modelling the interface conditions should be close to real considerations. Actually the interface between tunnel and rock is imperfect due to interstitial defaults like foliation, microcracks, mesoscale cavities, faults or joints at the interface and wall roughness. Moreover these discontinuities can be partially saturated with air or water and can thus modify the dissipation of the incoming energy. A few papers modelled imperfect interface with a linear spring [9,26] or a parallel linear dashpot and spring designs [27]. Indeed, imperfect bonding means here that the stress field is assumed to be continuous whereas the linear displacement field is not at the interface. The displacement jump is assumed to depend linearly on the traction vector, with potential normal and tangential component differences. The dependence can be real and frequency-independent (elastic spring case) or it may be complex and/or frequency-dependent (viscoelastic approach) [28]. Yi et al. investigated the frequency response of a circular tunnel with imperfect bonded interface in a full space elastic medium modelled with spring constants [9,26]. Fang and Jin proposed a viscoelastic interface model to study harmonic stress field around a non-circular tunnel in an elastic medium [27]. The viscoelastic imperfect boundary was modelled with a linear spring and a dashpot design.

The above literature review shows that the coupling of transient regimes and imperfect boundary conditions of lined tunnels seems to be absent. The novelty of this paper consists in studying at the same time transient regimes and imperfect bonded interfaces for simulating the dynamic response of a tunnel embedded in an elastic infinite rock. The subject of this paper thus focuses on the 2D transient response of a circular pipeline lying with an imperfect bonded contact in an elastic medium.

This paper is organized as follows. In section 2, a brief statement of the semi-analytical development is recalled. Details on the imperfect boundary conditions are precised. In section 3, the transient hoop stresses and displacements of both the tunnel and the rock are presented. Particularly, 2D snapshots of wave propagation in the rock and the lining are obtained for some parameters for which the effects of the imperfect interface can be observed and quantified. Indeed, the authors have noted that the displacement field in the tunnel is strongly modified and globally lower in comparison with the perfect case response.

2. Formulation

The two-dimensional problem configuration is illustrated in Fig. 1. A long cylindrical tunnel is embedded in an infinite rock medium. The outer radius of the tunnel is b and its inner radius is a. A transient incident P-wave propagates in the rock in the decreasing x axis direction and acts on the outer surface of the tunnel, as shown in Fig. 1.

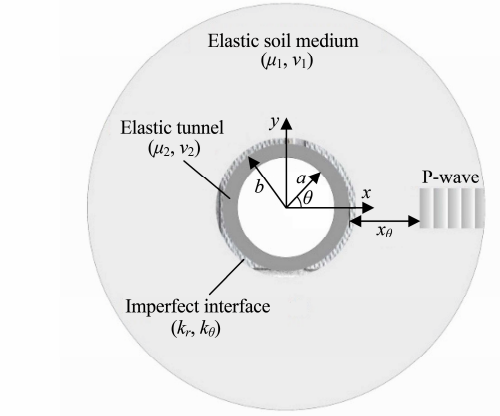

Fig. 1. Problem geometry.

2.1. Imperfect boundary conditions

Here an imperfect boundary condition hypothesis at the interface between the rock and the tunnel is assumed. Actually the interface zone can present various partially saturated discontinuities like foliation, microcracks, mesoscale cavities, faults or joints. These discontinuities can significantly impact the dynamic response of the tunnel. Even if this inhomogeneous area is quite difficult to apprehend, because it is mainly phenomenological and due to the intrinsic nature of the rock and the way the tunnel itself has been built, one of the most well-known models taking into account the imperfect boundary conditions is a two-linear-spring design: displacement field is assumed to be discontinuous along the entire length of the interface whereas traction field is assumed to be continuous. Applications of this concept do not exclusively concern seismic wave propagation but also non-destructive tests and natural or industrial composite materials. Relationships between experimental observations and the two-linear spring model can be found in [29-32], among others.

Based on this concept, the imperfect boundary conditions at the interface surface between the lining and the rock at $r=b$ can be written as follows [9,28,33].

$$\sigma_{rr1}=\sigma_{rr2},\sigma_{r\theta1}=\sigma_{r\theta2},\sigma_{rr1}=k_r(u_{r1}-u_{r2}),\sigma_{r\theta1}=k_\theta(u_{\theta1}-u_{\theta2}) \tag{1}$$

And the boundary conditions at the inner surface of the lining at $r=a$ are written as a free surface.

$$\sigma_{rr2}=0,\sigma_{r\theta2}=0 \tag{2}$$

where k_r and k_θ are the normal and tangential spring constants, respectively; $\mathbf{u}$ the displacement vector; and σ the stress tensor. Actually k_r and k_θ represent the roughness in radial and tangential directions respectively between rock and tunnel. Dividing the third equation in Eq. (1) by k_r or the fourth equation in Eq. (1) by k_θ, when these parameters tend to infinity, the left-hand sides tend to be zero, implying no jump in displacement between the tunnel and rock. This limit case represents thus the perfect continuity conditions; consequently, the perfect boundary conditions mean hereafter the largest values of k_r and k_θ. On the contrary, very low values of k_r and k_θ mean that traction efforts at the interface do not exist anymore.

2.2. Waves in rock and tunnel

The usual gradient and curve decomposition of the displacement vector, $\mathbf{u}=\nabla\phi+\nabla\times\Psi$, is used here leading to the following Helmholtz equations.

$$\nabla^2\phi=(1/c_p^2)(\partial^2\phi/\partial t^2),\nabla^2\Psi=(1/c_s^2)(\partial^2\Psi/\partial t^2) \tag{3}$$

where $c_p=\sqrt{(\lambda+2\mu)/\rho}$ and $c_s=\sqrt{\mu/\rho}$ are the P- and S-wave velocities in the elastic medium, respectively (where μ and λ are the Lamé constants and ρ is the material density). The displacement field $\mathbf{u}$ does not depend

on the z-coordinate due to the 2D studied configuration, so the vector potential Ψ only has one single component ψ_z. For simplicity it will be written as ψ. The Laplace transform defined by

$$\bar{f}(r,\theta,s)=\int_0^{\infty} f(r,\theta,t)e^{-st}dt \tag{4}$$

is then applied to Eq. (3).

The transient plane P-wave propagates in the rock in the negative x-direction, as shown in Fig. 1. The time variable is adjusted so that the incident wave front strikes the tunnel at $r=b$ and $\theta=0$ at $t=0$. The total scalar potential $\bar{\phi}_1^{\mathrm{t}}$, in the rock medium (subscript 1 denotes the wave features in the rock medium) and in the Laplace domain, is then composed of incident and refracted components as written in the following.

$$\bar{\phi}_1^{\mathrm{t}}=\underbrace{e^{-\bar{\alpha}_1 x_0}F(s)\sum_{n=0}^{\infty}\varepsilon_n I_n(\bar{\alpha}_1 r)\cos n\theta}_{\bar{\phi}^{\mathrm{i}},\ \text{incident wave}}+\underbrace{\sum_{n=0}^{\infty}A_n(s)K_n(\bar{\alpha}_1 r)\cos n\theta}_{\text{refracted P-wave}} \tag{5}$$

where $\bar{\alpha}_1=s/c_{p1}$ is the wavenumber of P-wave in the Laplace domain in the rock; x_0 the distance between the tunnel and incident wave before $t=0$; $F(s)$ an arbitrary excitation term expressed in the Laplace domain; $\varepsilon_n=1$ for $n=0$ and $\varepsilon_n=2$ for $n\geq 1$; K_n the modified Bessel function of the second kind of order n; and I_n the modified Bessel function of the first kind of order n.

Due to the interface between the rock and the tunnel, two refracted waves (P-wave as indicated in Eq. (5) and SV-wave in Eq. (6)) in the rock medium propagate when the incident wave acts on the outer surface of the tunnel. Since the scattering field vanishes when $r\to\infty$, they are represented by modified Bessel function of the second kind K_n [24]. Consequently, the total vector potential $\bar{\psi}_1^{\mathrm{t}}$, in the rock medium and in the Laplace domain, can be written as

$$\bar{\psi}_1^{\mathrm{t}}=\underbrace{\sum_{n=0}^{\infty}B_n(s)K_n(\bar{\beta}_1 r)\sin n\theta}_{\text{refracted SV-wave}} \tag{6}$$

where $A_n(s)$ and $B_n(s)$ are unknown coefficients; and $\bar{\beta}_1=s/c_{s1}$.

Also, for the tunnel medium (subscript 2) the scalar and vector potentials can be written as a combination of refracted and reflected waves as follows.

$$\bar{\phi}_2^{\mathrm{t}}=\sum_{n=0}^{\infty}[C_n(s)I_n(\bar{\alpha}_2 r)+D_n(s)K_n(\bar{\alpha}_2 r)]\cos n\theta \tag{7}$$

$$\bar{\psi}_2^{\mathrm{t}}=\sum_{n=0}^{\infty}[M_n(s)I_n(\bar{\beta}_2 r)+N_n(s)K_n(\bar{\beta}_2 r)]\sin n\theta \tag{8}$$

where $C_n(s)$, $D_n(s)$, $M_n(s)$ and $N_n(s)$ are unknown coefficients. From Eqs. (5)-(8), the potential decomposition of displacements, and the stress-strain relations, the displacement and stress components can be obtained everywhere in terms of the unknown coefficients. Then combining with the interface and boundary conditions, and with the use of the orthogonality properties, a matrix system can be written as

$$\mathbf{E}_n(s)\mathbf{Q}_n(s)=e^{-\bar{\alpha}_1 x_0}F(s)\in_n\mathbf{G}_n(s) \tag{9}$$

where $\mathbf{Q}_n(s)$ includes the unknown coefficients as follows.

$$\mathbf{Q}_n(s)=[A_n(s),B_n(s),C_n(s),D_n(s),M_n(s),N_n(s)]^t \tag{10}$$

And equations for $\mathbf{G}_n(s)$ and $\mathbf{E}_n(s)$ are shown as follows (see more details in [34]).

$$\mathbf{G}_n(s)=[\bar{\mu}e_3(\bar{\alpha}_1 b),\bar{\mu}e_5(\bar{\alpha}_1 b),e_1(\bar{\alpha}_1 b)-(2\mu_1/(bk_r))e_3(\bar{\alpha}_1 b),e_2(\bar{\alpha}_1 b)-(2\mu_1/(bk_\theta))e_5(\bar{\alpha}_1 b),0,0]^t \tag{11}$$

$$\mathbf{E}_n(s)=\begin{bmatrix} -\bar{\mu}e_{31}(\bar{\alpha}_1 b) & -\bar{\mu}e_{32}(\bar{\alpha}_1 b) & e_{33}(\bar{\alpha}_2 b) & e_{31}(\bar{\alpha}_2 b) & e_{34}(\bar{\alpha}_2 b) & e_{32}(\bar{\alpha}_2 b) \\ -\bar{\mu}e_{51}(\bar{\alpha}_1 b) & -\bar{\mu}e_{52}(\bar{\alpha}_1 b) & e_{53}(\bar{\alpha}_2 b) & e_{51}(\bar{\alpha}_2 b) & e_{54}(\bar{\alpha}_2 b) & e_{52}(\bar{\alpha}_2 b) \\ (2\mu_1/(bk_r))e_{31}(\bar{\alpha}_1 b)-e_{11}(\bar{\alpha}_1 b) & (2\mu_1/(bk_r))e_{32}(\bar{\alpha}_1 b)-e_{12}(\bar{\alpha}_1 b) & e_{13}(\bar{\alpha}_2 b) & e_{11}(\bar{\alpha}_2 b) & e_{14}(\bar{\alpha}_2 b) & e_{12}(\bar{\alpha}_2 b) \\ (2\mu_1/(bk_\theta))e_{51}(\bar{\alpha}_1 b)-e_{21}(\bar{\alpha}_1 b) & (2\mu_1/(bk_\theta))e_{52}(\bar{\alpha}_1 b)-e_{22}(\bar{\alpha}_1 b) & e_{23}(\bar{\alpha}_2 b) & e_{21}(\bar{\alpha}_2 b) & e_{24}(\bar{\alpha}_2 b) & e_{22}(\bar{\alpha}_2 b) \\ 0 & 0 & e_{33}(\bar{\alpha}_2 a) & e_{31}(\bar{\alpha}_2 a) & e_{34}(\bar{\alpha}_2 a) & e_{32}(\bar{\alpha}_2 a) \\ 0 & 0 & e_{43}(\bar{\alpha}_2 a) & e_{41}(\bar{\alpha}_2 a) & e_{44}(\bar{\alpha}_2 a) & e_{42}(\bar{\alpha}_2 a) \end{bmatrix} \tag{12}$$

where $\bar{\mu}=\mu_1/\mu_2$; and e_{ij} are given as follows.

$$\begin{aligned}
&e_1(\bar{\alpha}r)=nI_n(\bar{\alpha}r)+\bar{\alpha}rI_{n+1}(\bar{\alpha}r)\\
&e_{11}(\bar{\alpha}r)=nK_n(\bar{\alpha}r)-\bar{\alpha}rK_{n+1}(\bar{\alpha}r)\\
&e_{12}(\bar{\beta}r)=nK_n(\bar{\beta}r)\\
&e_{13}(\bar{\alpha}r)=nI_n(\bar{\alpha}r)+\bar{\alpha}rI_{n+1}(\bar{\alpha}r)\\
&e_{14}(\bar{\beta}r)=nI_n(\bar{\beta}r)\\
&e_2(\bar{\alpha}r)=-nI_n(\bar{\alpha}r)\\
&e_{21}(\bar{\alpha}r)=-nK_n(\bar{\alpha}r)\\
&e_{22}(\bar{\beta}r)=-nK_n(\bar{\beta}r)+\bar{\beta}rK_{n+1}(\bar{\beta}r)\\
&e_{23}(\bar{\alpha}r)=-nI_n(\bar{\alpha}r)\\
&e_{24}(\bar{\beta}r)=-nI_n(\bar{\beta}r)-\bar{\beta}rI_{n+1}(\bar{\beta}r)\\
&e_3(\bar{\alpha}r)=(n^2-n+\bar{\beta}^2r^2/2)I_n(\bar{\alpha}r)-\bar{\alpha}rI_{n+1}(\bar{\alpha}r)\\
&e_{31}(\bar{\alpha}r)=(n^2-n+\bar{\beta}^2r^2/2)K_n(\bar{\alpha}r)+\bar{\alpha}rK_{n+1}(\bar{\alpha}r)\\
&e_{32}(\bar{\beta}r)=n[(n-1)K_n(\bar{\beta}r)-\bar{\beta}rK_{n+1}(\bar{\beta}r)]\\
&e_{33}(\bar{\alpha}r)=(n^2-n+\bar{\beta}^2r^2/2)I_n(\bar{\alpha}r)-\bar{\alpha}rI_{n+1}(\bar{\alpha}r)\\
&e_{34}(\bar{\beta}r)=n[(n-1)I_n(\bar{\beta}r)+\bar{\beta}rI_{n+1}(\bar{\beta}r)]\\
&e_4(\bar{\alpha}r)=-(n^2-n-\bar{\beta}^2r^2/2+\bar{\alpha}^2r^2)I_n(\bar{\alpha}r)+\bar{\alpha}rI_{n+1}(\bar{\alpha}r)\\
&e_{41}(\bar{\alpha}r)=-(n^2-n-\bar{\beta}^2r^2/2+\bar{\alpha}^2r^2)K_n(\bar{\alpha}r)-\bar{\alpha}rK_{n+1}(\bar{\alpha}r)\\
&e_{42}(\bar{\beta}r)=n[(-n+1)K_n(\bar{\beta}r)+\bar{\beta}rK_{n+1}(\bar{\beta}r)]\\
&e_{43}(\bar{\alpha}r)=-(n^2-n-\bar{\beta}^2r^2/2+\bar{\alpha}^2r^2)I_n(\bar{\alpha}r)+\bar{\alpha}rI_{n+1}(\bar{\alpha}r)\\
&e_{44}(\bar{\beta}r)=n[(-n+1)I_n(\bar{\beta}r)-\bar{\beta}rI_{n+1}(\bar{\beta}r)]\\
&e_5(\bar{\alpha}r)=-n[(n-1)I_n(\bar{\alpha}r)+\bar{\alpha}rI_{n+1}(\bar{\alpha}r)]\\
&e_{51}(\bar{\alpha}r)=-n[(n-1)K_n(\bar{\alpha}r)-\bar{\alpha}rK_{n+1}(\bar{\alpha}r)]\\
&e_{52}(\bar{\alpha}r)=-(n^2-n+\bar{\beta}^2r^2/2)K_n(\bar{\beta}r)-\bar{\beta}rK_{n+1}(\bar{\beta}r)\\
&e_{53}(\bar{\alpha}r)=-n[(n-1)I_n(\bar{\alpha}r)+\bar{\alpha}rI_{n+1}(\bar{\alpha}r)]\\
&e_{54}(\bar{\alpha}r)=-(n^2-n+\bar{\beta}^2r^2/2)I_n(\bar{\beta}r)+\bar{\beta}rI_{n+1}(\bar{\beta}r)
\end{aligned} \tag{13}$$

Solving Eq. (9) for different values of $n\in[0,N]$, with N being the truncation constant of the infinite series, gives coefficients $A_n(s)$ … $N_n(s)$ and thus the displacement and stress fields everywhere in the Laplace domain.

2.3. Durbin's method

The inversion of Laplace transforms to obtain the transient responses is performed numerically by using the following Durbin's formula in the interval $[0,2T_0]$ [35,36].

$$\Lambda(t) = (2e^{ct}/T_0)[1/[2\,\mathrm{Re}[\bar{\Lambda}(c)]]] + \sum_{k=1}^{M}[\mathrm{Re}[\bar{\Lambda}(c + 2\pi ik/T_0)]\cos(2\pi kt/T_0) - \mathrm{Im}[\bar{\Lambda}(c + 2\pi ik/T_0)]\sin(2\pi kt/T_0)]] \tag{14}$$

where M is the truncation parameter; and c an arbitrary real number. $\Lambda(s)$ can be any of $\bar{u}_r(s)$, $\bar{u}_\theta(s)$, $\bar{\sigma}_{rr}(s)$, $\bar{\sigma}_{\theta\theta}(s)$. The suggested value of cT_0 and M are between 5-10, and 50-5,000 for sufficient accuracy, respectively [35].

3. Numerical results

3.1. Validation

To validate our development, and due to the lack of transient response when taking into account an imperfect boundary scenario, a comparison is proposed with the frequency approach of Yi et al. [9]. The comparison concerns the harmonic response of a tunnel embedded in an elastic rock subjected to incident plane compressional wave.

Fig. 2 presents the dynamic stress concentration factor $\sigma^*_{\theta\theta}$ of the rock at r=b, recalled by

$$\sigma^*_{\theta\theta} = |\sigma_{\theta\theta}/\sigma_0| \tag{15}$$

where $\sigma_0 = \mu_1\beta_1^2\phi_0$ with ϕ_0 the amplitude of the incident wave. The hoop stress is considered here since, in cylindrical tunnel configurations, it is bigger than radial or axial stresses. The rock and lining parameters in Fig. 2 are taken directly from Yi et al.: ν_1=0.25, ν_2=0.3, μ_1/μ_2=0.31, c_{p1}/c_{p2}=0.7, b/a=1.2 and $\alpha_1 a$=2 [9]. The same three different values of k_r and k_θ are also considered. Excellent agreement between present results and those from [9] is obtained.

Second, in order to show the reliability of transient response, a cylindrical cavity in the elastic medium under a step load acting on the inner surface of the cavity is considered and compared to [37]. The following nondimensional parameters have been chosen: ν_1=ν_2=0.3, μ_1/μ_2=1, c_{p1}/c_{s1}=c_{p2}/c_{s2}=√3.5, b/a=1.2, c_{s1}/c_{s2}=1 and k_r=k_θ=100μ_1/b. A big value for the spring constant at the interface between the rock and the lining changes the imperfect boundary condition to a perfect interface, as discussed previously. Good agreement is obtained, as shown in Fig. 3, for the mode of the displacement (n=0) and at points (r=a, θ=0).

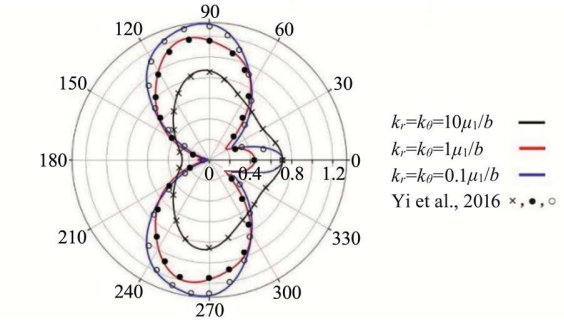

Fig. 2. Comparison of dimensionless hoop stress of the present results and results of [9] in the rock for different values of k_r and k_θ.

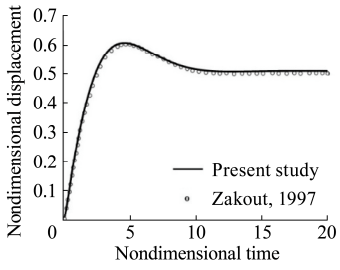

Fig. 3. Comparison of the nondimensional displacement of rock without shell as a function of the nondimensional time for n=0 with results of [37].

3.2. Main results

Mechanical values (tunnel and rock parts) are given in Table 1 from Fang and Jin [27]. The outer and inner radius of the tunnel are b=1 m and a=0.8 m.

Table 1 Material properties for the rock and tunnel.

Parameters	Rock	Tunnel
ρ (kg/m^3)	2,730	2,500
E (GPa)	35	30
ν	0.3	0.25
μ (GPa)	13.462	12
λ (GPa)	20.192	12
c_p (m/s)	4,154.3	3,794.7
c_s (m/s)	2,220.6	2,190.9
c_p^*	1	0.9134
c_s^*	0.5345	0.5274

Results are obtained for the following dimensionless quantities.

$$u^* = u/b, \sigma_{\theta\theta}^* = \sigma_{\theta\theta}/\rho_1 c_{p1}^2, t^* = c_{p1}t/b, c_{p1}^* = 1, c_{p2}^* = c_{p2}/c_{p1}, c_{s1}^* = c_{s1}/c_{p1}, c_{s2}^* = c_{s2}/c_{p1} \tag{16}$$

The incident plane wave in the Laplace domain in Eq. (5) is chosen as $F(s)=1/(s+3)$, and the corresponding time expression is $f(t^*)=e^{-3t^*}$. Durbin's formula is evaluated with M=1,200, $c=5/T_0$ and T_0=60.

Fig. 4 displays the dimensionless hoop stress of the rock $\sigma_{\theta\theta 1}^*$ at ($r=b$, θ=0 and $\pi/2$) and the tunnel $\sigma_{\theta\theta 2}^*$ at ($r=a$, θ=0 and $\pi/2$) for the same three different values of imperfect boundary condition coefficients. Recall that perfect conditions are modelled with the highest values of k_r and k_θ as explained previously, corresponding here to the black curves in Fig. 4. The dimensionless hoop stress in the rock at ($r=b$, θ=0) is increased when tending towards the perfect bond configuration. On the contrary, for ($r=b$, $\theta=\pi/2$) the dimensionless hoop stress is slightly larger for the weak bond (blue curves). Actually this fact has been observed in the harmonic response studied by Yi et al. who showed the complicated effects of k_r and k_θ with respect to θ [9]. Consequently it cannot be asserted that the displacement or stress fields are larger in the perfect case for every θ, even if the overall response for perfect boundary conditions clearly presents higher amplitudes. By increasing the value of k_r and k_θ the dimensionless hoop stresses of the tunnel in both points are strongly increased (lower figures) due to the higher level of wave transmission. The most important point here concerns the oscillating feature of the dynamic response of the tunnel, and to a lower extent of the rock, when the perfectly bonded interface conditions are considered. On the contrary, for very low values of k_r and k_θ, or highly imperfect boundary conditions, the materials are detached from each other and tunnel does not affect rock response significantly. Actually, the response of the rock is similar to the case without tunnel (dashed lines).

Values of $k_r=k_\theta=1\mu_1/b$ lead to intermediate responses for both the tunnel and the rock (see red curves in Fig. 4). Since the dimensionless P-wave velocities in rock and tunnel are $c_{p1}^*=1$ and $c_{p2}^*=0.91$ respectively, the elastic wave arrives sooner in the rock in comparison with the tunnel. Also, a short delay in the response of the tunnel at ($r=a$, θ=0) can be seen due to the thickness of the tunnel.

Fig. 5 exhibits the dimensionless radial displacements of the rock u_{r1}^* at ($r=b$, θ=0 and $\pi/2$) and the tunnel u_{r2}^* at ($r=a$, θ=0 and $\pi/2$) for the same three different values of imperfect boundary condition coefficients. Observations mentioned for Fig. 4 are confirmed for the displacement analysis concerning the influence of the boundary conditions on the amplitude of the response and on the oscillating behaviour. For instance, for θ=0 the nondimensional displacement in tunnel (left lower sub-figure) shows differences up to several hundred percent between cases $k_r=k_\theta=10\mu_1/b$ and $k_r=k_\theta=1\mu_1/b$ (black and red curves respectively). This illustrates the fact that the incoming energy for weak contact is consumed between tunnel and rock due to rough interface, and that the tunnel receives less energy. A pseudo-periodicity around $T^*\approx 2\times(0.2/0.91)\approx 0.44$ due to the multiple reflections in the tunnel and specifically for the perfect bonded case is also observed.

Figs. 6 and 7 are analogous to Figs. 4 and 5 respectively but for a 0.4 m tunnel lining thickness (b=1 m, a=0.6 m). The main difference concerns the oscillations: the pseudo-period is doubled due to the thickness of the lining. The amplitudes are not so much perturbed and the boundary condition type impacts the mechanical fields in a similar trend.

Figs. 8-11 exhibit the nondimensional displacement snapshots of the rock and the tunnel for various selected times, for perfect and imperfect boundary conditions, for a 0.2 m lining thickness (Figs. 8 and 9) and a 0.4 m lining thickness (Figs. 10 and 11). Fig. 12 presents the snapshots relative to the case of the rock without lining. The plane wave front is clearly seen and is deformed when it impacts the tunnel surface. In the perfect boundary condition cases, the nondimensional displacement of the tunnel is larger in comparison with the imperfect cases. As mentioned in section 2.2, concerning the imperfect boundary conditions, discontinuities and faults between the tunnel and the rock behave like a barrier against the input energy of incident wave. The multiple reflections in the tunnel, discussed in Figs. 4 and 5, are thus observed in the perfect contact configurations, leading to disturbed fields. In the imperfect cases, the displacement field in the tunnel is smoother. No notable difference in rock displacement is noticed.

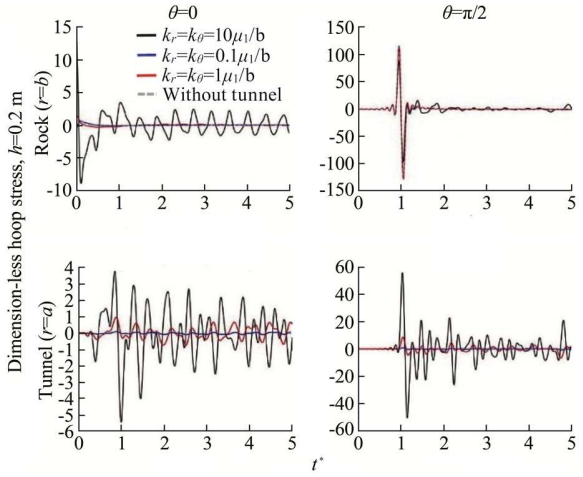

Fig. 4. Dimensionless hoop stresses of rock and tunnel for θ=0 and π/2, different ratios of k_r and k_θ and a 0.2 m lining thickness.

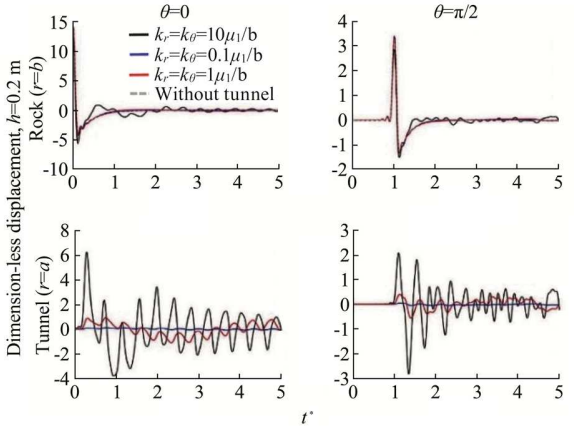

Fig. 5. Dimensionless radial displacements of rock and tunnel for θ=0 and π/2, different ratios of k_r and k_θ and a 0.2 m lining thickness.

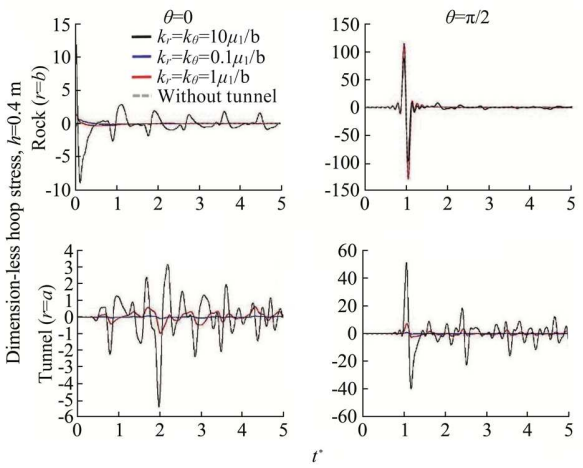

Fig. 6. Dimensionless hoop stresses of rock and tunnel for θ=0 and π/2, different ratios of k_r and k_θ and a 0.4 m lining thickness.

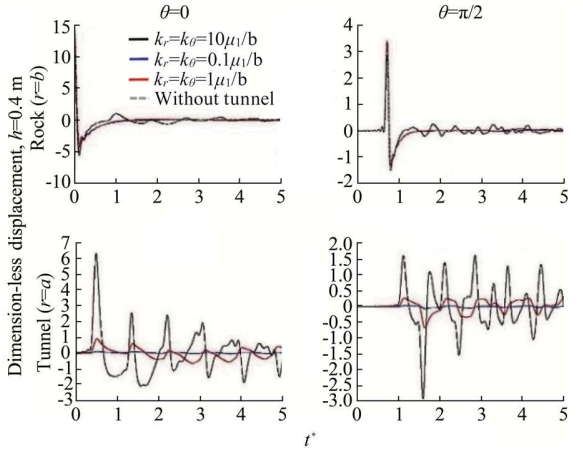

Fig. 7. Dimensionless radial displacements of rock and tunnel for θ=0 and π/2, different ratios of k_r and k_θ and a 0.4 m lining thickness.

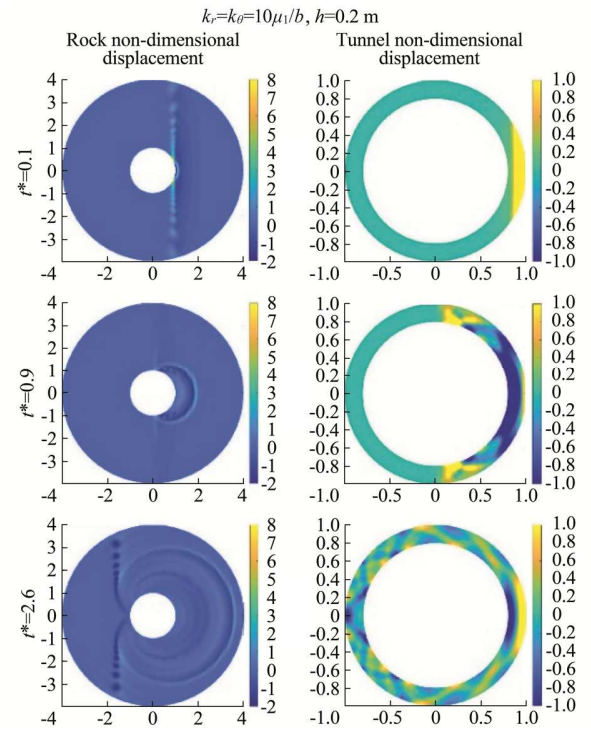

Fig. 8. Dimensionless displacement snapshots of rock and tunnel for large value of k_r and k_θ (perfect interface case) for selected times and for a 0.2 m lining thickness.

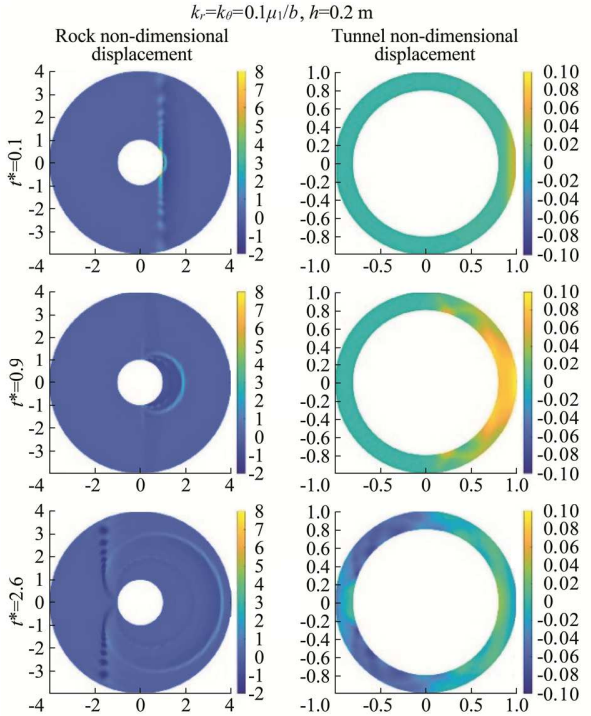

Fig. 9. Dimensionless displacement snapshots of rock and tunnel for small value of k_r and k_θ (imperfect interface case) for selected times and for a 0.2 m lining thickness.

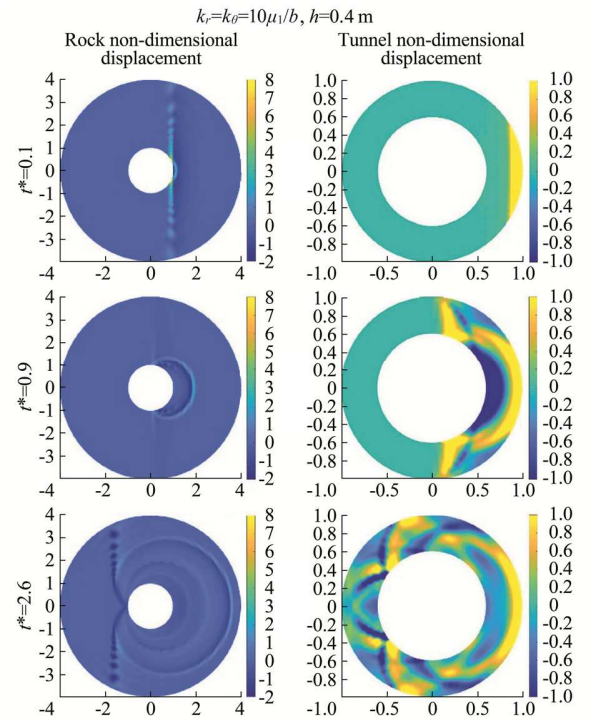

Fig. 10. Dimensionless displacement snapshots of rock and tunnel for large value of k_r and k_θ (perfect interface case) for selected times and for a 0.4 m lining thickness.

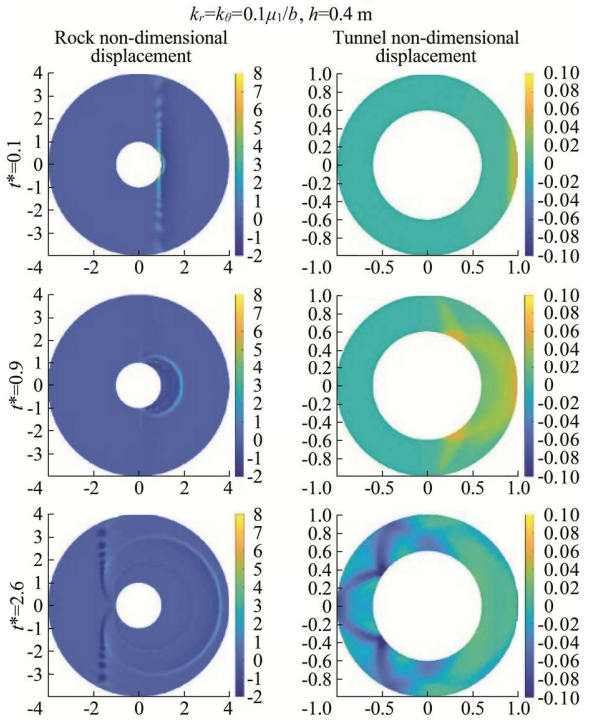

Fig. 11. Dimensionless displacement snapshots of rock and tunnel for small value of k_r and k_θ (imperfect interface case) for selected times and for a 0.4 m lining thickness.

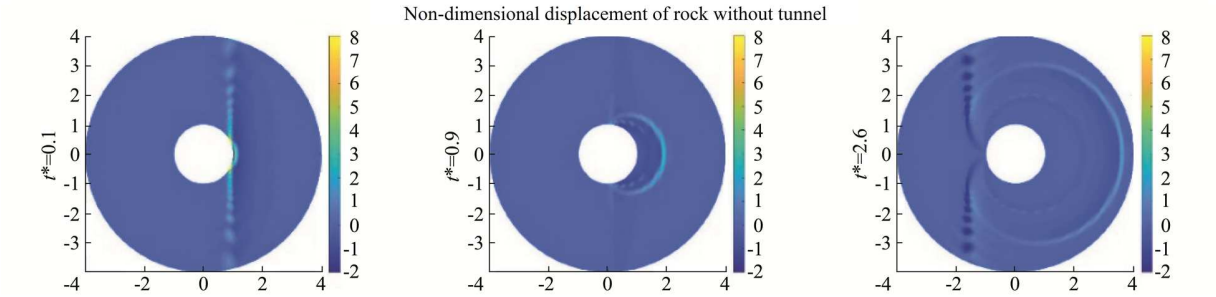

Fig. 12. Dimensionless displacement snapshots of rock without lining for selected times.

4. Conclusion

In this paper, the 2D transient response of an imperfect bonded circular lined pipeline lying in an elastic infinite medium has been obtained. Imperfect interaction surface between elastic medium and tunnel has been considered as a two-linear-spring model. The elastodynamic wave equations of P- and S-waves have been solved in the Laplace domain, using Helmholtz decompositions and Bessel and Hankel series expressions. Durbin's numerical Laplace transform inversion approach has been used to obtain transient responses.

The global dynamic semi-analytical development has been validated by comparison with previous results. Indeed, the closed form solution in this study paves the way for future to optimize the mid-layer properties in order to get the acceptable dynamic stress around the underground structures for any type of wave loading. The influences of imperfect conditions on both the dynamic hoop stresses and displacements of the tunnel and rock have been analyzed. The tunnel behavior is greatly impacted by the nature of the interface. Perfect bond interface configurations have shown oscillating features in the responses of the tunnel. Weak bond interface configurations have led to low overall level of dynamic responses. No significant effect on the displacement of the rock has been observed.

Further works will consider from the theoretical point of view both the implementation and the sensitivity study of a damaged zone area and its specific contact with the tunnel and the rock, and the development of anisotropic and/or porous characteristics of both the lining and the external environment. From the experimental point of view, specific results extracted directly from the Low Noise Inter-Disciplinary Underground Science and Technology Laboratory will be compared, after data treatment, to simulation results.

Acknowledgements

This work has been carried out under a PhD grant from Conseil Général Provence-Alpes-Côte d'Azur, France. This support is gratefully acknowledged. The authors also wish to express their gratitude to Stéphane Gaffet, Head of the Low Noise Inter-Disciplinary Underground Science and Technology Laboratory for his constructive comments during this project.

References

[1] Beres J. Characterisation of anisotropy in a karstified carbonate plateform using seismic and electrical resistivity methods: a joint approach. Doctoral dissertation. Paris: University Paris Sud; 2013.
[2] Mesgouez A, Buis S, Lefeuve-Mesgouez G, Micolau G. Use of global sensitivity analysis to assess the soil poroelastic parameter influence. Wave Motion 2017;72:377-94.
[3] Virieux J, Operto S. An overview of full-waveform inversion in exploration geophysics. Geophysics 2009;74(6):WCC127-52.
[4] Lefeuve-Mesgouez G, Mesgouez A, Ogam E, Scotti T, Wirgin A. Retrieval of the physical properties of an anelastic solid half space from seismic data. Journal of Applied Geophysics 2013;88:70-82.
[5] Mesgouez A. Characterization of a viscoelastic heterogeneous object with an effective model by nonlinear full waveform inversion. Journal of Sound and Vibration 2018;422:189-209.
[6] Sidler R, Carcione JM, Holliger K. A pseudo-spectral method for the simulation of poro-elastic seismic wave propagation in 2D polar coordinates using domain decomposition. Journal of Computational Physics 2013;235:846-64.
[7] Zhou XL, Wang JH, Xu B, Jiang LF. Dynamic response of a circular pipeline in a poroelastic medium. Mechanics Research Communications 2009;36(8):898-905.

[8] Gao M, Wang Y, Gao GY, Yang J. An analytical solution for the transient response of a cylindrical lined cavity in a poroelastic medium. Soil Dynamics and Earthquake Engineering 2013;46:30-40.
[9] Yi CP, Lu WB, Zhang P, Johansson D, Nyberg U. Effect of imperfect interface on the dynamic response of a circular lined tunnel impacted by plane P-waves. Tunnelling and Underground Space Technology 2016;51:68-74.
[10] Manolis GD, Tetepoulidis PI, Talaslidis DG, Apostolidis G. Seismic analysis of buried pipeline in a 3D soil continuum. Engineering Analysis with Boundary Elements 1995;15(4):371-94.
[11] Clouteau D, Arnst M, Al-Hussainia TM, Degrande G. Freefield vibrations due to dynamic loading on a tunnel embedded in a stratified medium. Journal of Sound and Vibration 2005;283(1-2):173-99.
[12] Tadeu AJB, Kausel E, Vrettos C. Scattering of waves by subterranean structures via the boundary element method. Soil Dynamics and Earthquake Engineering 1996;15(6):387-97.
[13] Karakostas CZ, Manolis GD. Dynamic response of unlined tunnels in soil with random properties. Engineering Structures 2000;22(8):1013-27.
[14] Tadeu AJB, Antonioa JMP, Kausel E. 3D scattering of waves by a cylindrical irregular cavity of infinite length in a homogeneous elastic medium. Computer Methods in Applied Mechanics and Engineering 2002;191(27-28):3015-33.
[15] Panji M, Kamalian M, Asgari Marnani J, Jafari MK. Transient analysis of wave propagation problems by half-plane BEM. Geophysical Journal International 2013;194(3):1849-65.
[16] Alielahi H, Kamalian M, Adampira M. Seismic ground amplification by unlined tunnels subjected to vertically propagating SV and P waves using BEM. Soil Dynamics and Earthquake Engineering 2015;71:63-79.
[17] Kouretzis GP, Bouckovalas GD, Gantes CJ. Analytical calculation of blast-induced strains to buried pipelines. International Journal of Impact Engineering 2007;34(10):1683-704.
[18] Feldgun VR, Kochetkov AV, Karinski YS, Yankelevsky DZ. Internal blast loading in a buried lined tunnel. International Journal of Impact Engineering 2008;35(3):172-83.
[19] Smerzini C, Avilés J, Paolucci R, Sánchez-Sesma FJ. Effect of underground cavities on surface earthquake ground motion under SH wave propagation. Earthquake Engineering and Structural Dynamics 2009;38(12):1441-60.
[20] Anh VTT, Bich DH, Duc ND. Nonlinear stability analysis of thin FGM annular spherical shells on elastic foundations under external pressure and thermal loads. European Journal of Mechanics, A/Solids 2015;50:28-38.
[21] Dinh Duc N, Dinh Nguyen P, Dinh Khoa N. Nonlinear dynamic analysis and vibration of eccentrically stiffened S-FGM elliptical cylindrical shells surrounded on elastic foundations in thermal environments. Thin-Walled Structures 2017;117:178-89.
[22] Kim SE, Duc ND, Nam VH, Van Sy N. Nonlinear vibration and dynamic buckling of eccentrically oblique stiffened FGM plates resting on elastic foundations in thermal environment. Thin-Walled Structures 2019;142:287-96.
[23] Kouretzis GP, Andrianopoulos KI, Sloan SW, Carter JP. Analysis of circular tunnels due to seismic P-wave propagation, with emphasis on unreinforced concrete liners. Computers and Geotechnics 2014;55:187-94.
[24] Zhai C, Xia T, Du G, Ding Z. Dynamic response of cylindrical cavity to antiplane impact load by using analytical approach. Journal of Central South University 2014;21(1):405-15.
[25] Fu J, Liang J, Qin L. Dynamic soil-tunnel interaction in layered half-space for incident P-and SV-waves. Earthquake Science 2015;28(4):275-84.
[26] Yi CP, Zhang P, Johansson D, Nyberg U. Dynamic response of a circular lined tunnel with an imperfect interface subjected to cylindrical P-waves. Computers and Geotechnics 2014;55:165-71.
[27] Fang XQ, Jin HX. Visco-elastic imperfect bonding effect on dynamic response of a non-circular lined tunnel subjected to P and SV waves. Soil Dynamics and Earthquake Engineering 2016;88:1-7.
[28] Schoenberg M. Elastic wave behavior across linear slip interfaces. Journal of the Acoustical Society of America 1980;68(5):1516-21.
[29] Honarvar F. Nondestructive Evaluation of Cylindrical Components by Resonance Acoustic Spectroscopy. Doctoral dissertation. Toronto: University of Toronto; 1997.
[30] Lourme H. Etude des assemblages collés par ondes guides ultrasonores: étude expérimentale et modélisation par éléments finis. Doctoral dissertation. Bordeaux: University of Bordeaux; 2009.
[31] Vlasie V, de Barros S, Rousseau M, Champaney L, Duflo H, Morvan B. Mechanical and acoustical study of a structural bond: comparison theory/numerical simulations/experiment. European Journal of Mechanics, A/Solids 2006;25(3):464-82.
[32] Valier-Brasier T, Dehoux T, Audoin B. Scaled behavior of interface waves at an imperfect solid-solid interface. Journal of Applied Physics 2012;112(2):024904.
[33] Achenbach JD. Wave propagation in elastic solids. North-Holland; 2005.
[34] Shakeri R, Mesgouez A, Lefeuve-Mesgouez G. Dynamic response of a circular tunnel with imperfect surface interaction embedded in an elastic medium. In: Proceedings of the 23rd French Mechanics Congress. Lille; 2017.
[35] Durbin F. Numerical Inversion of Laplace Transforms: An Efficient Improvement to Dubner and Abate's Method. Computer Journal 1974;17(4):371-6.
[36] Hasheminejad SM, Shakeri R, Rezaei S. Vibro-acoustic response of an elliptical plate-cavity coupled system to external shock loads. Applied Acoustics 2012;73(8):757-69.
[37] Zakout U, Akkas N. Transient response of a cylindrical cavity with and without a bonded shell in an infinite elastic medium. International Journal of Engineering Science 1997;35(13-12):1203-20.